



Supplement of

Future changes in atmospheric rivers over East Asia under stratospheric aerosol intervention

Ju Liang and Jim Haywood

Correspondence to: Ju Liang (j.liang@exeter.ac.uk)

The copyright of individual parts of the supplement might differ from the article licence.

Model verification

Here we evaluate the performance of UKESM1 in simulating the historical climatology of ARs over East Asia using two historical climate datasets. The simulated AR features by UKESM1 are evaluated by comparing with those identified in the Fifth Generation ECMWF Atmospheric Reanalysis (ERA5, Hersbach et al., 2020). ERA5 is based on the 4D-Var data assimilation technique and a spectral GCM at a spectral horizontal resolution of $\sim 0.25^\circ$ with 137 vertical levels. ERA5 has been used in studies on the historical long-term trends in ARs and the relationship between ARs and large-scale atmospheric circulation over East Asia (Pan and Lu 2020; Park et al., 2021; Liang et al., 2022; Liang and Yong, 2022). As Liang and Yong (2022), the AR-associated precipitation is diagnosed using gridded daily precipitation data from the Asia Precipitation—Highly Resolved Observational Data Integration Towards Evaluation of Water Resources (APHRODITE v1101, Yatagai et al. 2014). The horizontal resolution of the data is 0.25° . The data is produced by interpolating in-situ rain gauge data using an angular-distance-weighting method to consider the relationship between local topography and precipitation (Yatagai et al. 2014) and addressing the inhomogeneity and error in rain-gauge measurements using an automated quality control system (Hamada et al. 2011).

Comparisons between the simulated AR characteristics in UKESM1 and those identified in ERA5 and APHRODITE shows that UKESM1 is capable of representing the historical pattern of ARs and the associated environmental fields of different levels in East Asia with respect to ERA5 (Figure S1). Though some biases are noted, including: overestimated (underestimated) AR frequency (Figure S1c) and the mean and extreme precipitation (Figure S2) in the upstream (downstream) region; an overestimated strength of the southwesterly monsoonal flow and the westerly jet stream during the main AR season (May to September, MJJAS); underestimations of the fractional contributions of ARs to annual total precipitation and extreme precipitation (Figure S3). However, the simulated patterns from UKESM1 displayed some similarities to those in ERA5

and APHRODITE, including the concentrated AR activity across 25° N (Figure S1a, b) that leads to relatively high AR-associated mean and extreme precipitation across Southern China, the Korean Peninsula and Japan (Figure S2). In addition, UKESM1 reasonably captures the negative correlations between AR frequency and the strength of westerly jet stream in terms of the East Asian Jet Stream Index (EAJSI) to the north of 35° N compared to the ERA5 reanalysis dataset (Figure S4a, b), though underestimation of such a correlation is observed to the east of 135° E (Figure S4c) and this bias is partly related to the underestimated AR frequency over the downstream region (Figure S1c). Overall, comparisons between the UKESM1 simulation and historical climate data indicate some reliability of the information on the impact of SAI on ARs provided by the model.

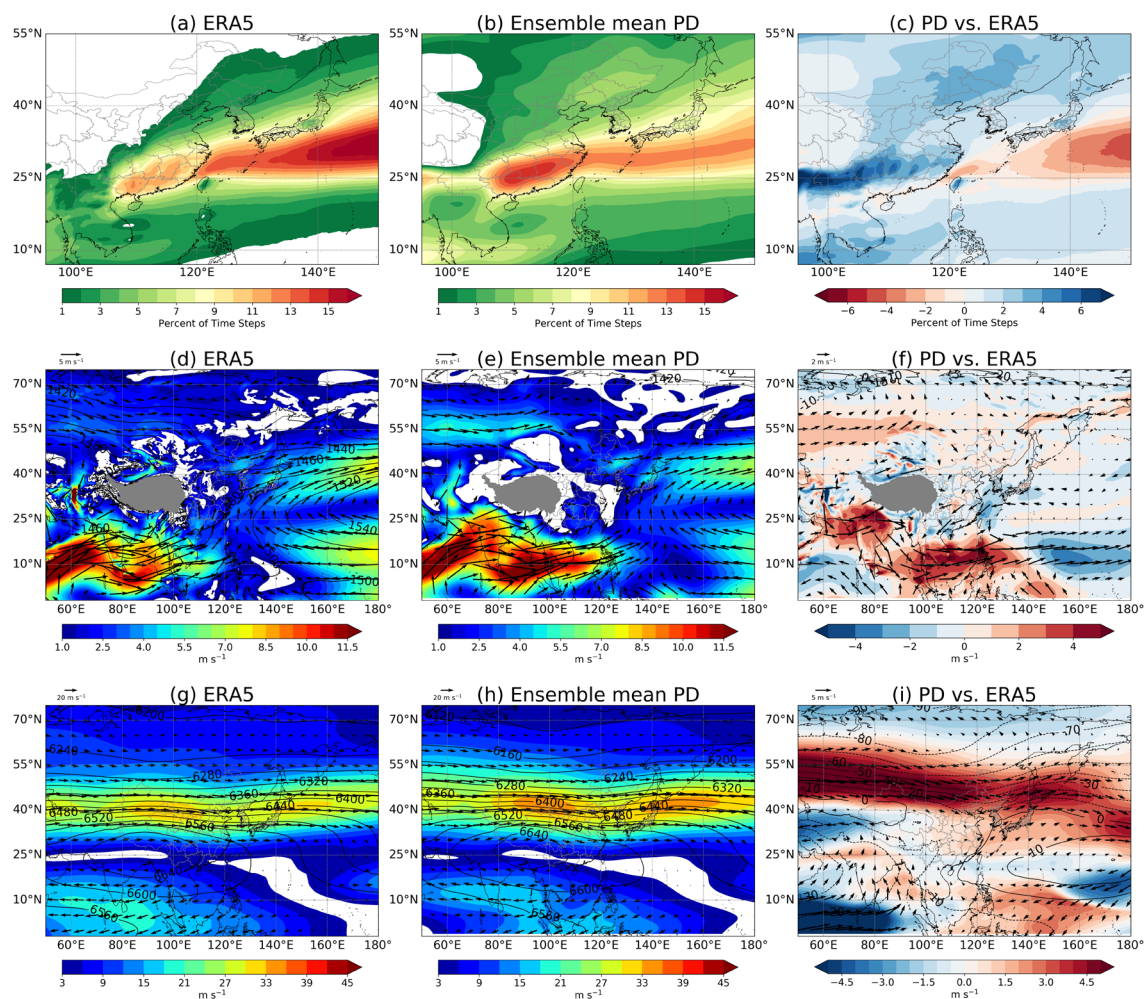


Fig. S1. Analyses of the detected AR features and AR-associated environmental fields for the period 1981-2010 from ERA5 (a, d, g), the ensemble mean of UKESM1 (b, e, h) and the biases for the UKESM1 ensemble mean relative to ERA5 (c, f, i): (a-c) AR frequency; (d-f) MJJAS-mean 850-hPa winds (shaded: wind speed; vectors: direction) and geopotential height (black contours); (g-i) MJJAS-mean 200-hPa winds

(shaded and vectors) and geopotential thickness between 200-500 hPa (black contours). Gray regions in d-f depict the Tibetan Plateau where the surface pressure is likely below 850-hPa.

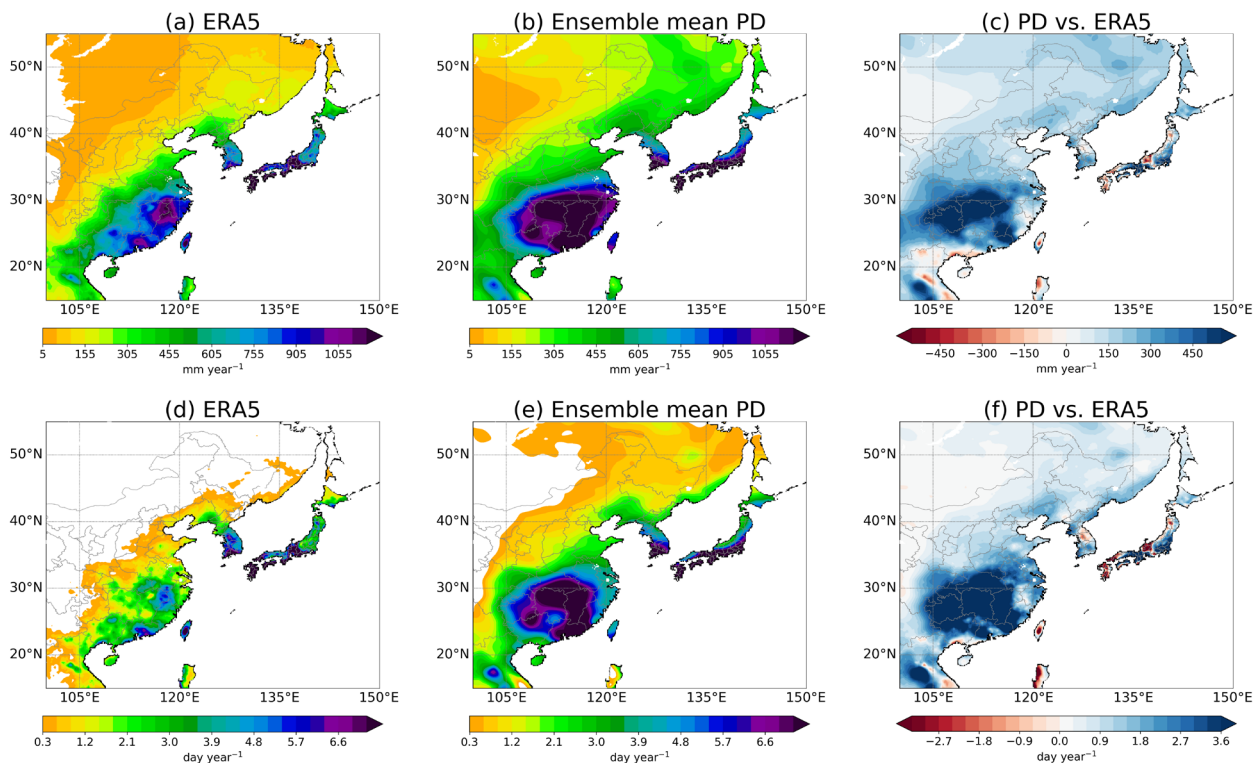


Fig. S2. Distributions of AR-associated precipitation (a-c) and heavy rain events (d-f) for the period 1981-2010: (a, d) ERA5; (b, e) the ensemble mean of UKESM1; the biases for the UKESM1 ensemble mean relative to ERA5.

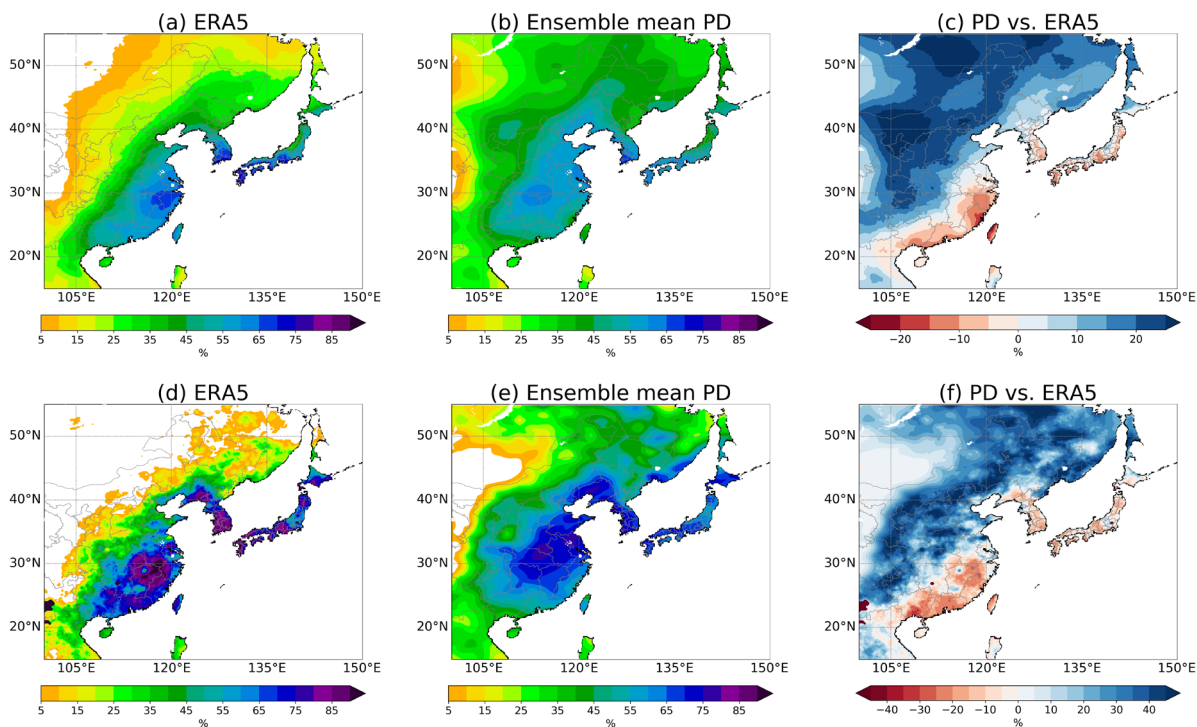


Fig. S3. As Figure S2, but for the fractional contributions of ARs relative to the annual total precipitation and heavy rain events.

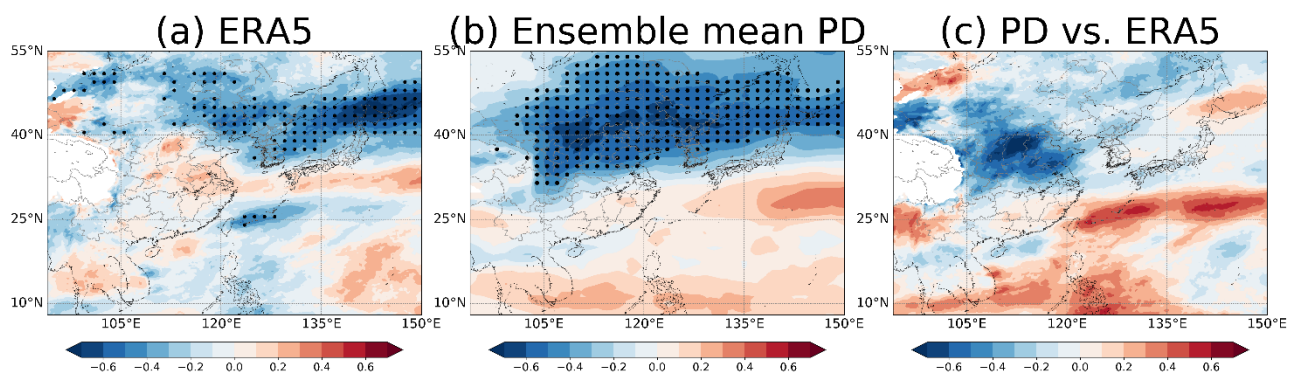


Fig. S4. Distributions of correlation coefficients between the annual AR frequency and MJJAS-mean EAJSI for the present-day simulations during the period 1981-2010 in ERA5 (a) and UKESM1 (b). Absolute differences between UKESM1 and ERA5 are shown in (c). Stippling in (a, b) indicates correlations that are statistically significant at a confidence level of $> 95\%$ (p -value < 0.05). EAJSI is calculated monthly as the difference between the monthly mean 200-hPa zonal wind speed averaged over the region $30\text{--}40^\circ\text{ N}$, $120\text{--}150^\circ\text{ E}$ and that over $40\text{--}50^\circ\text{ N}$, $120\text{--}150^\circ\text{ E}$ following Lu et al. (2011).

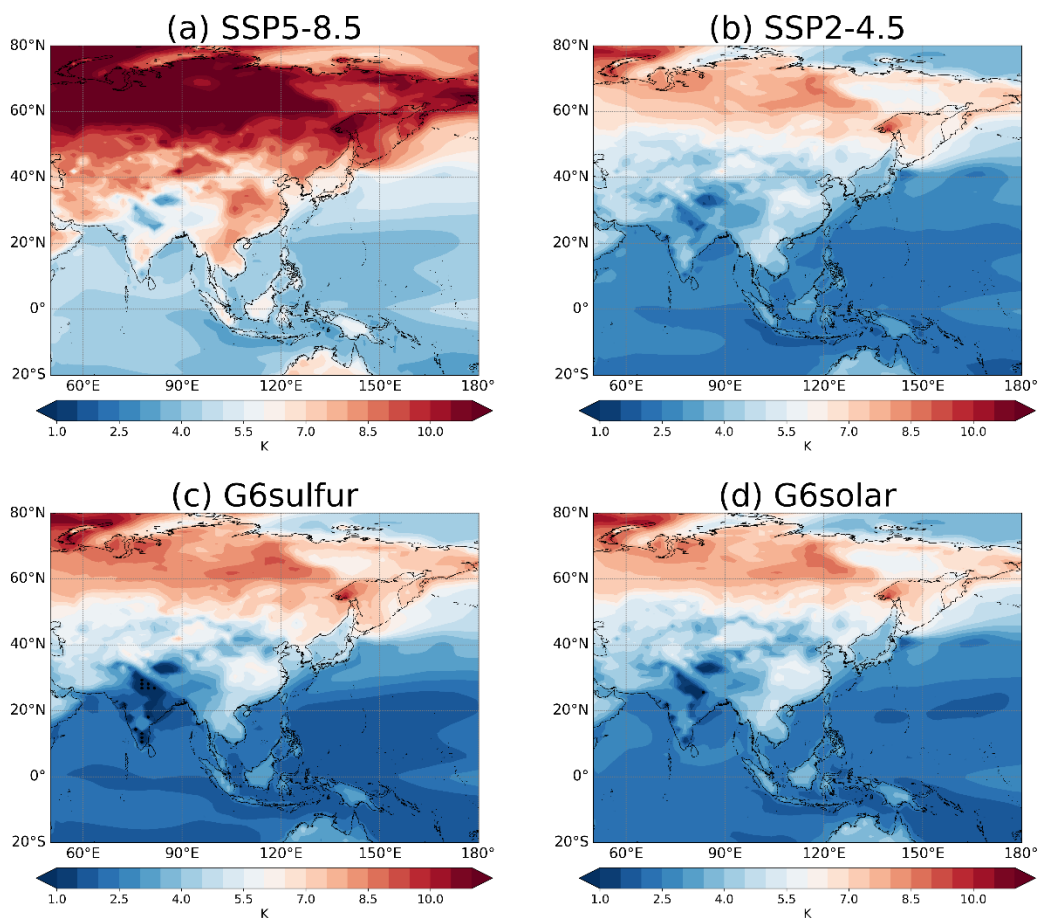


Fig. S5. Absolute changes in MJJAS-mean surface temperature for the future period of 2071-2100 relative to the historical baseline during 1981-2010.

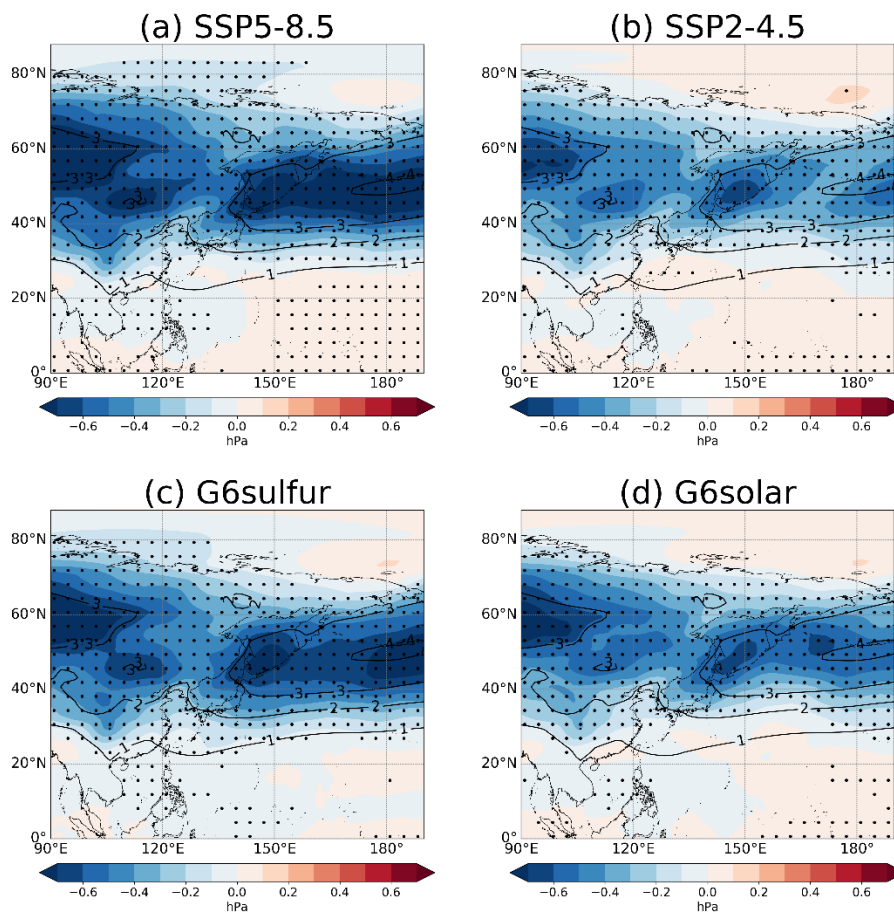


Fig. S6. Absolute changes in the root-mean-square of 2-6-day bandpass-filtered MSLP (unit: hPa) distribution during MJJAS for the future period of 2071-2100 relative to the historical baseline during 1981-2010. Black contours show the distribution during the historical baseline period. Stippling indicates changes that are statistically significant at a confidence level of $> 95\%$ (p -value < 0.05 based on the Student's t -test).

References

- Hamada, A., Arakawa, O., and Yatagai, A.: An automated quality control method for daily rain-gauge data, *Glob. Environ. Res.*, 15, 183–192, 2011.
- Hersbach, H., Bell, B., Berrisford, P., Hirahara, S., Horányi, A., Muñoz-Sabater, J., Nicolas, J., Peubey, C., Radu, R., Schepers, D., Simmons, A., Soci, C., Abdalla, S., Abellan, X., Balsamo, G., Bechtold, P., Biavati, G., Bidlot, J., Bonavita, M., De Chiara, G., Dahlgren, P., Dee, D., Diamantakis, M., Dragani, R., Flemming, J., Forbes, R., Fuentes, M., Geer, A., Haimberger, L., Healy, S., Hogan, R. J., Hólm, E., Janisková, M., Keeley, S., Laloyaux, P., Lopez, P., Lupu, C., Radnoti, G., de Rosnay, P., Rozum, I., Vamborg, F., Villaume, S., and Thépaut, J. N.: The ERA5 global reanalysis, *Q. J. R. Meteorol. Soc.*, 146, 1999–2049, <https://doi.org/10.1002/qj.3803>, 2020.
- Liang, J., Yong, Y., and Hawcroft, M. K.: Long-term trends in atmospheric rivers over East Asia, *Clim. Dyn.* 2022, 1–24, <https://doi.org/10.1007/S00382-022-06339-5>, 2022.
- Liang, J. and Yong, Y.: Sensitivity of the simulated atmospheric rivers over East Asia to horizontal resolution in the HadGEM3-GC3.1 general circulation model, *Atmos. Res.*, 275, 106244, <https://doi.org/10.1016/j.atmosres.2022.106244>, 2022.
- Lu, R., Ye, H., and Jhun, J. G.: Weakening of interannual variability in the summer East Asian upper-tropospheric westerly jet since the mid-1990s, *Adv. Atmos. Sci.*, 28, 1246–1258, <https://doi.org/10.1007/s00376-011-0222-5>, 2011.

Pan, M. and Lu, M.: East Asia atmospheric river catalog: Annual cycle, transition mechanism, and precipitation, *Geophys. Res. Lett.*, 47, 1–10, <https://doi.org/10.1029/2020GL089477>, 2020.

Park, C., Son, S. W., and Kim, H.: Distinct Features of Atmospheric Rivers in the Early Versus Late East Asian Summer Monsoon and Their Impacts on Monsoon Rainfall, *J. Geophys. Res. Atmos.*, 126, e2020JD033537, <https://doi.org/10.1029/2020JD033537>, 2021.

Yatagai, A., Krishnamurti, T. N., Kumar, V., Mishra, A. K., and Simon, A.: Use of APHRODITE rain gauge-based precipitation and TRMM 3B43 products for improving asian monsoon seasonal precipitation forecasts by the superensemble method, *J. Clim.*, 27, 1062–1069, <https://doi.org/10.1175/JCLI-D-13-00332.1>, 2014.